 CMES, vol.1, no.4, pp.1-22, 2012

A model of the spatially dependent mechanical properties of the axon during its growth

J.A. García[1,2], J.M. Peña[1], S. McHugh[2] and A. Jérusalem[2]

Abstract: Neuronal growth is a complex process involving many intra- and extracellular mechanisms which are collaborating conjointly to participate to the development of the nervous system. More particularly, the early neocortical development involves the creation of a multilayered structure constituted by neuronal growth (driven by axonal or dendritic guidance cues) as well as cell migration. The underlying mechanisms of such structural lamination not only implies important biochemical changes at the intracellular level through axonal microtubule (de)polymerization and growth cone advance, but also through the directly dependent stress/stretch coupling mechanisms driving them. Efforts have recently focused on modeling approaches aimed at accounting for the effect of mechanical tension or compression on the axonal growth and subsequent soma migration. However, the reciprocal influence of the biochemical structural evolution on the mechanical properties has been mostly disregarded. We thus propose a new model aimed at providing the spatially dependent mechanical properties of the axon during its growth. Our in-house finite difference solver *Neurite* is used to describe the guanosine triphosphate (GTP) transport through the axon, its dephosphorylation in guanosine diphosphate (GDP), and thus the microtubules polymerization. The model is calibrated against experimental results and the tensile and bending mechanical stiffnesses are ultimately inferred from the spatially dependent microtubule occupancy. Such additional information is believed to be of drastic relevance in the growth cone vicinity, where biomechanical mechanisms are driving axonal growth and pathfinding. More specifically, the confirmation of a lower stiffness in the distal axon ultimately participates in explaining the controversy associated to the tensile role of the growth cone.

Keywords: Microtubule polymerization, mechanical properties, axonal growth,

[1] DATSI Computer Science, Universidad Politécnica de Madrid, Campus de Montegancedo, 28860 Madrid, Spain

[2] IMDEA Materials Institute, C/ Profesor Aranguren, 28840 Madrid, Spain; corresponding author: antoine.jerusalem@imdea.org

finite difference modeling

1 Introduction

Neuronal growth and migration such as the ones observed during neocortical development, and more generally during plasticity (Pascual-Leone, Amedi, Fregni, and Merabet, 2005), involve a complex collaboration between the intracellular biomechanical mechanisms (e.g., microtubule polymerization, lamellipodia and filipodia formation) and the potential extracellular mechanical and chemical stimuli (e.g., contact forces, guidance cues). Different families of computational models have been proposed with the objective of understanding the internal dynamics of these processes, as well as obtaining records that are technically impossible—or at least very difficult—to achieve by experimental means. To this end, the large diffusion of electrophysiological packages such as *Genesis* (Bower and Beeman, 1998) or *Neuron* (Carnevale and Hines, 2006) has permitted the simulation of electrical propagation in many types of neuronal networks. However, in such frameworks, the neuron distribution remains spatially static. Evolving neuronal morphological models, on the other hand, are not only much scarcer but also generally avoid the coupling of the biomechanically evolving structure to its electrophysiological response. To date, one of the most general computational frameworks is CX3D (Zubler and Douglas, 2009). This framework provides a three-dimensional model of neuronal network growth and migration, accounting for the pushing, pulling and contact forces of all neurons. However, it does not explicitly spatially differentiate the mechanical properties within each neurite, i.e., the influence of the chemical mechanisms on the mechanical properties is not accounted for. Among others, CX3D qualitatively simulates cue guidance, intracellular diffusion and chemical reactions, neocortical lamination, growth of neocortical pyramidal cell and neural network formation by neurite fasciculation (Zubler and Douglas, 2009).

Various models have also been previously proposed (generally tackling only some of these phenomena), most of them based on microtubule polymerization and/or growth cone advance as drivers for neurite elongation (Graham and van Ooyen, 2006). Such models normally involve the production, degradation, transport and transformation of several molecules within each neurite at three different stages: neuritogenesis, axonogenesis and dendritogenesis, linked together by sequences of branching and elongations (Poulain and Sobel, 2010). Neuritogenesis has been modeled by considering the competition of neurites within the same neuron (van Ooyen, Graham, and Ramakers, 1994). Focusing on the elongation stages, a family of models has been proposed by directly associating neurite elongation to microtubules assembly at the tip of the neurite with production, transportation and diffusion of tubulin dimers from the soma (van Veen and van Pelt, 1994; McLean,

van Ooyen, and Graham, 2004; Graham, Lauchlan, and Mclean, 2006). Another family of models is simulating the outgrowth of branching in neurites by considering the dynamic mechanical behavior of the growth cone under biochemical stimuli (van Veen and van Pelt, 1992; Li, Qin, and Wang, 1995; Aeschlimann, 2000; Krottje and van Ooyen, 2007) or internal chemical secretion and transport (Graham and van Ooyen, 2001, 2004). Alternatively, branching modeling has been approached by stochastic means (van Pelt, Dityatev, and Uylings, 1997; van Pelt and Schierwagen, 2004). The decreasing velocity of the motor proteins during axonal transport away from the cell body (Miller and Samuels, 1996), as well as the effect of microtubule associated proteins group 2 (MAP2) (de)phosphorylation on microtubule consolidation (Hely, Graham, and van Ooyen, 2001) have also been accounted for. Finally, different models of microtubule dynamic instability have been proposed (Jobs, Wolf, and Flyvbjerg, 1997; Hammele and Zimmermann, 2003; Margolin, Gregoretti, Goodson, and Alber, 2006; Janulevicius, van Pelt, and van Ooyen, 2006).

In parallel to these efforts, other research groups have modeled the mechanical properties of individual axons (Dennerll, Joshi, Steel, Buxbaum, and Heidemann, 1988; Dennerll, Lamoureux, Buxbaum, and Heidemann, 1989; Bernal, Pullarkat, and Melo, 2007; Ouyang, Nauman, and Shi, 2010a). Using such models, mechanical tension has been proposed as a stimulator of axonal elongation and retraction (Heidemann and Buxbaum, 1994). Growth cones, on the other hand, have been characterized as poor "tractors" (Lamoureux, Buxbaum, and Heidemann, 1998), limiting microtubule polymerization driven axonal outgrowth. Microtubule polymerization thus arises as a propelling mechanical system (Dogterom and Yurke, 1997; Dogterom, Kerssemakers, Romet-Lemonne, and Janson, 2005) at the source of many of the characteristics of axonal pathfinding (Tanaka and Kirschner, 1991; Williamson, Gordon-Weeks, Schachner, and Taylor, 1996; Gordon-Weeks, 2004).

Despite the fact that a knowledge of the axonal mechanical properties appears as particularly relevant (especially in the vincinity of the axon tip), a polymerization based spatially dependent model of the axonal mechanical properties is still missing. The model we propose here aims at filling this gap. The complex intertwinned relation between the growth cone advance and microtubule polymerization is still a subject of debate (Dent and Gertler, 2003). As a first approximation, the growth is thus assumed to be exclusively microtubule polymerization driven (McLean, van Ooyen, and Graham, 2004). Guanosine triphosphate (GTP) bound tubulin dimers are produced in the cell body, based on the observation that, under normal circumstances, axons lack the synthesis machinery for internal GTP tubulin dimers production (Twiss and Fainzilber, 2009). As a second step, the dimers are transported from the soma to the axon tip by two different mechanisms: diffusion and

active transport. In view of the important controversy on the active transport of full sections of polymerized microtubule (Glabraith, Reese, Schlief, and Gallant, 1999; Baas and Buster, 2004; Ma, Shakiryanova, Vardya, and Popov, 2004), this phenomenon is discarded as a first approximation (only dimers are transported). Following polymerization of concurrent microtubules within each axonal element, the mechanical properties of the overall axon are ultimately calculated based on microtubule occupancy. The calculations are done with our dedicated finite difference solver *Neurite*.

The overall approach is described in detail in Section 2. The finite difference discretization scheme is then briefly described in Section 3 and the results, validated against experimental results, are given in Section 4 and discussed in Section 5. A conclusion to this work is finally proposed in Section 6.

2 Methods

The cell cytoskeleton is an adaptable crosslinked network composed, among others, by actin filaments, intermediate filaments and microtubules. These internal structural components work together to provide mechanical strength to the cell. Along with the dynamic actin-supported structure placed at the tip of the axon called the growth cone, microtubules are the main structural components of the neurites (Dent and Gertler, 2003). This intertwinned relation between the microtubules and the growth cone is responsible for axonal steering and, ultimately, sypnase creations with neighboring neurons (axonal pathfinding). It is thus necessary to characterize the mechanical properties of the axon during its growth at the tip to better understand the push/pull/contact relationship between the axon and the neighboring tissue, and its effect on the axonal pathfinding processes.

Microtubules are polarized hollow tubes formed by guanosine diphosphate (GDP) tubulin dimers dephosphorylated from GTP. The associated dynamic instability of this (de)phosphorylation is at the source of the microtubules capability to reorganize and adapt to the cell evolution needs (Kirschner and Mitchinson, 1986). Most of the polymerization (with faster growth) occurs at one end of the polarized microtubule called "+-end" (Hawkins, Mirigian, Yasar, and Ross, 2010). Inside the axon, the microtubules form a parallel bundled array and their +-ends point uniformaly towards the axon tip, whereas, in dendrites, the microtubules have a mixed orientation, some pointing towards the cell body and others towards the dendritic tip (Conde and Cáceres, 2009).

We focus here on the axon, in which the GTP tubulin dimers are transported through diffusion and motor protein active transport. At the microtubules tips, the GTP dimers are dephosphorylated in GDP dimers, thus polymerizing the microtubules,

see Fig. 1. As branching is not accounted for in this 1D model, the effect of microtubule severing proteins such as katanin or spastin (Conde and Cáceres, 2009) is not taken into account. The influence of MAP2/tau family microtubule associated proteins (MAPs) on the microtubules structural integrity will be added to the model in future works.

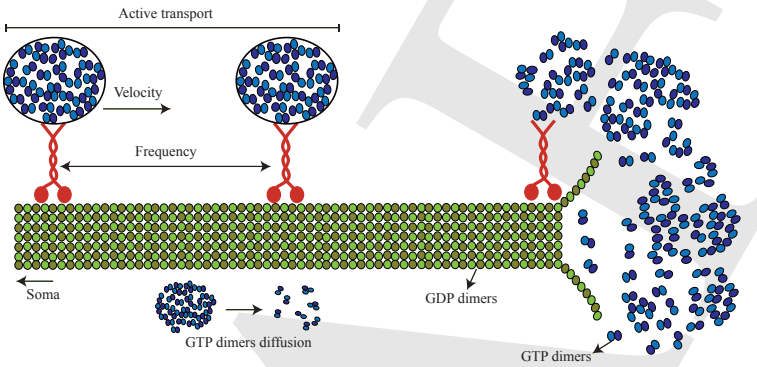

Figure 1: Overall model scheme: GTP tubulin dimers are transported by diffusion and active transport, and are dephosphorylated at the tip into GDP tubulin dimers, the microtubule building blocks

2.1 GTP tubulin dimers transport

It is assumed here that the tubulin dimers are produced exclusively in the cell body. Note however that observations of local protein synthesis have been reported, mostly after axonal damage, but that the complementary contribution of ribosomal proteins from other neighboring cells was suggested as an explanation (Twiss and Fainzilber, 2009; F. Bradke and Spira, 2012). Based on previous findings, diffusion is known to govern the axonal growth at short range (proximal), whereas active transport governs the outgrowth at long range (distal), assumed here to occur at a constant slow transport rate (Glabraith, Reese, Schlief, and Gallant, 1999).

2.1.1 Diffusion

The diffusion process is assumed to follow Fick's law along the 1D x-axis representative of the axonal path:

$$J = -D\frac{\partial [GTP]}{\partial x} \tag{1}$$

where J is the flux (positive from high to low concentrations), D the diffusion coefficient, and $[GTP]$ the concentration of GTP tubulin dimers at coordinate x. Note that the diffusion coefficient is assumed constant. This approximation could be relaxed by accounting for all the smaller scale organelles, proteins, etc. populating the axoplasm and participating to the effective diffusion; such complexity is however out of the scope of the proposed model. Fick's second law then states that the rate of concentration is directly proportional to the spatial derivative of J:

$$\frac{\partial [GTP]}{\partial t} = D \frac{\partial^2 [GTP]}{\partial x^2} \tag{2}$$

Finally, a constant GTP tubulin dimer concentration is assumed in the soma.

2.1.2 Active tranport

We assume here a constant active anterograde transport velocity (Glabraith, Reese, Schlief, and Gallant, 1999) from the soma to the +-ends of the polymerizing microtubules. This assumption is motivated by the fact that the advancement of the motor proteins is driven by the hydrolysis of adenosine triphosphate, in turn assumed evenly distributed in the axoplasm. When a motor protein reaches the microtubule tip, it releases its GTP tubulin dimers vesicle, thus making them available for diffusion or dephosphorylation. For each microtubule inside the axon, the model monitors the positions of all associated motor proteins, and updates them at each time step based on their velocity:

$$V = \frac{dx_k}{dt} \tag{3}$$

where V is the active transport velocity for all motor proteins, and x_k the coordinate of motor protein k.

Note that active transport is not considered until a threshold axonal length is reached. This condition is physically rationalized by the fact that the differentiation of the axon vs. dendrites is a non-immediate process, eventually concluded by a global reorientation of the microtubules +-ends away from the soma (Poulain and Sobel, 2010; Lindsley, Kerlin, and Rising, 2003). This process indicates that anterograde active transport mechanisms are indeed not immediately available in the axon.

2.1.3 GTP to GDP dephosphorylation

In a neighborhood of the microtubule +-ends, the dephosphorylation of GTP to microtubule bound GDP is simplified as follows:

$$[GTP] \underset{k_2}{\overset{k_1}{\rightleftharpoons}} [GDP] \tag{4}$$

where k_1 and k_2 characterize the reaction rates of dephosphorylation (microtubule assembly) and phosphorylation (microtubule disassembly), respectively. In order to reduce the model parameter space, we assume as a first approximation that $k_2 = 0$ (this assumption will be relaxed in future extensions of the model, e.g., to model the pathological causes of cell necrosis). Eq. 4 thus yields:

$$\frac{\partial [GDP]}{\partial t} = k_1 [GTP] \tag{5}$$

Adding depolymerization to this model would obviously permit a more realistic simulation of the growth intrinsic mechanisms (Flyvbjerg, Jobs, and Leibler, 1996; McLean, van Ooyen, and Graham, 2004; Janulevicius, van Pelt, and van Ooyen, 2006), as well as the determination of "oscillation instability thresholds" (Jobs, Wolf, and Flyvbjerg, 1997; Hammele and Zimmermann, 2003). However, the set of equations involved in such models would invariably lead to a much larger space of parameters whose determination is out of the scope of this work. The mechanical model proposed in the following can however be adapted straightforwardly to these other models.

2.2 Mechanical modeling

As discussed in Section 1, it is now widely accepted that the push/pull/contact mechanical constraints with the surrounding tissue in the neighborhood of the growth cone is an important driver of axonal growth and/or pathfinding. The goal of this work is thus to propose a methodology aimed at complementing existing finite difference or compartmental models with mechanical properties prediction of the axon during its growth. To this end, we propose to evaluate the overall mechanical properties of the axon by identifying the individual contributions of the GDP tubulin dimers (microtubule building blocks) and the surrounding membrane, see Fig. 2.

Both the overall membrane and each one of the microtubules have a hollow section of area S_m and S_μ, and a Young's modulus of E_m and E_μ, respectively. Their elastic behavior can then be idealized by a set of springs put in parallel (see Fig. 2), and characterized by their constants k_m and k_μ following:

$$k_i = \frac{E_i S_i}{L}, \forall i \in \{m, \mu\} \tag{6}$$

The force F necessary to elongate by ΔL an axonal element of initial length L is thus the sum of the forces in all its internal components. This statement is equivalent to considering that Eq. 6 also applies to the overall cylindrical axon element with an equivalent Young's modulus E_a, section area S_a, and spring constant k_a.

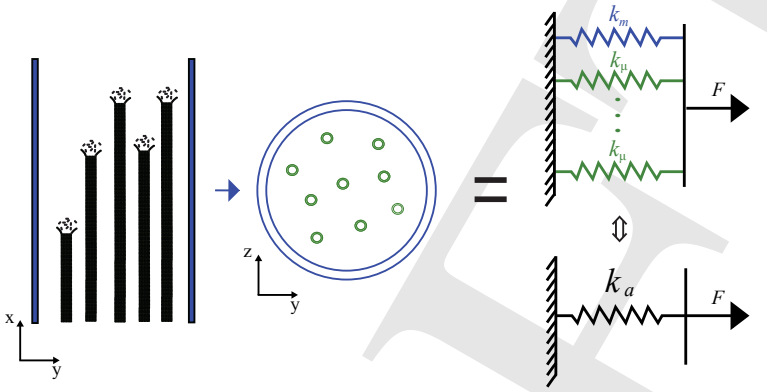

Figure 2: Mechanical model: the axon section is constituted by microtubules and membrane; their stiffnesses k_μ and k_m act in parallel, leading to an overall equivalent axonal stiffness k_a

Noting that:

$$\begin{cases} S_\mu = \pi(r_{\mu+}^2 - r_{\mu-}^2) \\ S_m \approx 2\pi r_a h_m \\ S_a = \pi r_a^2 \end{cases} \tag{7}$$

where $r_{\mu+}$, $r_{\mu-}$, r_a and h_m are respectively the external and internal microtubule radii, the axon radius and the membrane thickness, and that the number of polymerized microtubules for a given axonal element is given by:

$$n_\mu = \frac{[GDP]S_a}{\alpha} \tag{8}$$

where α is the number of GDP tubulin dimers per unit length of polymerized microtubule (function of the tubulin dimer length and the number of circumferencial dimers in microtubules), and where $[GDP]$ is the concentration of GDP tubulin dimers (embedded in microtubules) in the considered axonal element; the equivalent axonal Young's modulus is thus given by:

$$E_a = \frac{2h_m}{r_a}E_m + \frac{\pi[GDP](r_{\mu+}^2 - r_{\mu-}^2)}{\alpha}E_\mu \tag{9}$$

The equivalent bending stiffness of the axonal element K_a can then be calculated by use of the area moment of inertia of hollow cylinders (for the membrane and

each microtubule), following the bending counterpart of Fig. 2:

$$K_a = \pi r_a^3 h_m E_m + \frac{\pi^2 r_a^2 [GDP](r_{\mu+}^4 - r_{\mu-}^4)}{4\alpha} E_\mu + \pi(r_{\mu+}^2 - r_{\mu-}^2) E_\mu \sum_\mu d_\mu^2 \tag{10}$$

where the sum of all squares of distances d_μ between the centers of each microtubule and the bending axis passing through the cross-section center of the axon element can be approximated as follows:

$$\sum_\mu d_\mu^2 \approx n_\mu < d_\mu^2 >= \frac{\pi r_a^2 [GDP]}{\alpha} \int_0^{r_a} \int_0^{2\pi} (r\sin\theta)^2 \frac{r d\theta dr}{\pi r_a^2} = \frac{\pi r_a^4 [GDP]}{4\alpha} \tag{11}$$

assuming that the microtubules are uniformally distributed within the axon.

3 Finite difference discretization

Our dedicated finite difference solver, *Neurite*, was used to solve explicitely the system of equations formed by Eq. 2, Eq. 3, and Eq. 5. A microtubule occupancy model was coupled to this scheme to define the amount of microtubules per element.

3.1 Discretized scheme

In this explicit scheme, the system is discretized spatially (subsequently, i superscript) and temporally (subsequently, n subscript). The discretization of the system thus reads:

$$\begin{cases} [GTP]_i^{n+1} = [GTP]_i^n + \frac{\Delta t D}{\Delta x^2}\left([GTP]_{i-1}^n - 2[GTP]_i^n + [GTP]_{i+1}^n\right) \\ x_k^{n+1} = x_k^n + \Delta t V \\ [GDP]_i^{n+1} = [GDP]_i^n + \Delta t k_1 [GTP]_i^n \end{cases} \tag{12}$$

where Δt is the time step and Δx is the finite difference element size of the discretized axon.

3.2 Microtubule occupancy model

The finite difference domain is chosen larger than the domain of study such that the axonal length is simply defined by the last element with a non-null microtubule occupancy.

When a motor protein reaches its microtubule tip, its cargo is released inside the current element. In the first element, microtubule "m+1" will begin its polymerization

only once microtubule "m" reaches the next element. In the other elements, a microtubule will undergo polymerization only as a continuation of the previous element. Finally, for all elements, a maximum number of microtubules is allowed. This number is considered here as a model parameter. Note that its value (arbitrarily chosen here as 50) is known to depend on the type of neuron and animal, and generally ranges between 10 and 100 (Peter and Mofrad, 2012). The overall mechanism is illustrated in Fig. 3, and the number of microtubules for a given element is given by Eq. (8)[1].

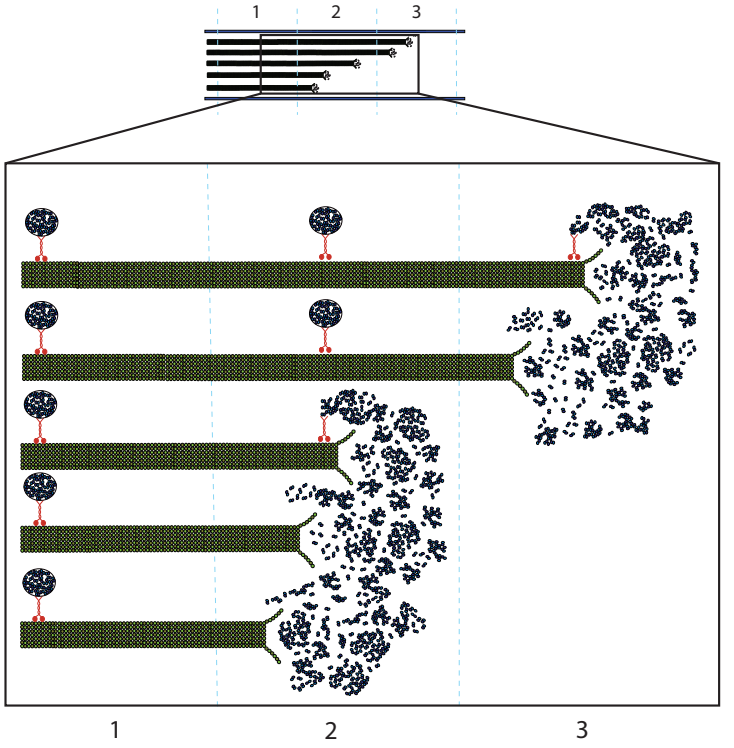

Figure 3: Active transport finite difference scheme of the discretized axon: motor proteins travel from the soma along microtubules; their cargos are then released in their respective elements for further diffusion and/or dephosphorylation

[1] Note that the number is not an integer in this case based on the assumption that even a portion of microtubule participates to the stiffnesses of the element.

3.3 Temporal and spatial convergences

A spectral analysis of Eq. 12 yields the following stability condition:

$$\Delta t \leq \Delta t_{critical} = \frac{\Delta x^2}{2D} \tag{13}$$

By taking $\Delta t = 0.1\Delta t_{critical}$, temporal convergence was observed for all calculations. The way the spatial scheme is designed limits however the spatial convergence. Indeed, polymerization, through Eq. 4, is function of the concentration of GTP dimers, which in turn involves different number of dimers for different element sizes. This intrinsic size dependence thus implies the consideration of a "distance of influence", around the tip of a polymerizing microtubule, whose GTP dimers will be the only ones involved in the polymerization. An element size of $1\mu m$ was chosen as representative of this distance of influence. A non-local approach assuming cargo delivery in the neighboring elements as a function of the time step and element size will be adopted in future models to avoid this issue.

4 Results

Our model is calibrated against experimental axonal growth measurements of an embryonic rat hippocampal neuron (Lindsley, Kerlin, and Rising, 2003). The model parameters are given in Tables Tab. 1 and Tab. 2. The first table lists the parameters that could be extracted from the literature, whereas the latter table shows the remaining parameters that had to be calibrated.

Note that the parameters given in Table 1 are not all defined for the hippocampal region (when not universal). This is the case of the maximum number of microtubules per axon, the active transport velocity and the diffusion coefficient. However all three values are by nature difficult to estimate, and are generally proposed as within a range, such as for the maximum number of microtubules (Peter and Mofrad, 2012), or for a reference idealized cell, such as for the active transport velocity and diffusion (Keith, 1987; Graham, Lauchlan, and Mclean, 2006). Based on the absence of more precise values in the literature, these values were taken by default.

Finally, as can be seen in Table 2, the model consists of only five free parameters, namely the axonal length threshold for active transport, the time between two motor protein emissions, the vesicle GTP dimer cargo, the GTP tubulin dimers concentration in the soma, and the polymerization rate constant.

4.1 Axonal growth

Upon calibration, a good agreement is obtained between the experimental (Lindsley, Kerlin, and Rising, 2003) and simulation results, see Fig. 4. It must be empha-

Table 1: Model parameters extracted from literature data

Parameter	Value	Reference
Axon radius (r_a)	$\sim 0.8\mu m$	Lee, Bashur, Gomez, Goldstein, and Schmidt (2010)
Membrane thickness (h_m)	$4nm$	Koch (1999)
Internal microtubule radius ($r_{\mu-}$)	$8nm$	Conde and Cáceres (2009)
External microtubule radius ($r_{\mu+}$)	$12nm$	Conde and Cáceres (2009)
Tubulin dimer length	$8nm$	Hawkins, Mirigian, Yasar, and Ross (2010)
Number of circumferencial dimers in microtubules	13	Hawkins, Mirigian, Yasar, and Ross (2010)
Maximum number of microtubules per axon	50	Peter and Mofrad (2012)
Membrane Young's modulus (E_m)	$1kPa$	McGarry and Prendergast (2004)
Microtubule Young's modulus (E_μ)	$1.9GPa$	Suresh (2007)
Active transport velocity (V)	$\sim 100\mu m.h^{-1}$	Keith (1987)
Diffusion coefficient (D)	$8.33 \times 10^{-12} m^2.s^{-1}$	Graham, Lauchlan, and Mclean (2006)

Table 2: Calibrated parameters

Parameter	Value
Axonal length threshold for active transport	$20\mu m$
Time between two motor protein emissions	2.49 hours
Vesicle GTP dimer cargo	$8 \times 10^{-20} mol$
GTP tubulin dimers concentration in the soma	$3 \times 10^{-5} mol.m^{-3}$
Polymerization rate constant (k_1)	$1.27 s^{-1}$

sized that four of the five free parameters have been observed to affect the growth curve independently. The axonal length threshold for active transport affects the departure from the first growth phase, i.e. during axonal differentiation (Lindsley, Kerlin, and Rising, 2003); the time between two motor protein emissions, the interval time between two polymerization activity peaks; the vesicle cargos, the intensity

of these peaks; and the GTP tubulin dimer concentration in the soma, the slope of the curve during the differentiation phase. However, the polymerization rate constant affects the overall slope of the curve (including the differentiation phase). By retaining the parameters within reasonable range, one possible fit is proposed here. More efforts to characterize independently all the parameters are needed.

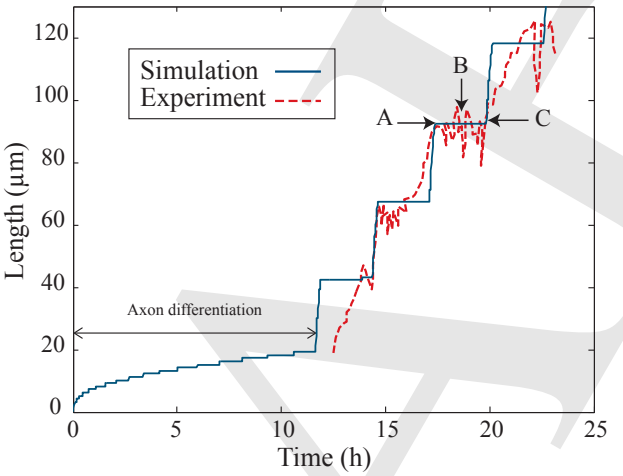

Figure 4: Calibrated simulation vs. experimental growth curve (Lindsley, Kerlin, and Rising, 2003); A: tip position at $62,700s$, B at $65,780s$, and C at $71,500s$

In the first phase of the curve, diffusion is governing the growth whereas active transport is mainly responsible for the second phase. The overall oscillation corresponding in the model to the arrival of a vesicle at the tip of the microtubules seems to be responsible for the low frequency oscillations of the experimental results. Note that the rapid depolymerization/polymerization oscillations (high frequency) experimentally observed are not modeled here. These results are especially remarkable considering the fact that the free parameters have been reduced to the very minimum in our simulations.

4.2 Mechanical properties

We now focus our mechanical properties study on states A, B and C in Fig. 4. The framework presented in Section 2.2 is applied to these states in order to evaluate the mechanical properties of the axon. The results are shown in Fig. 5. The observation of the number of microtubules in each element shows that the axon has reached full microtubule occupancy (50) for the first $86\mu m$ of axon. At the axon tip however

($86\mu m$ to $93\mu m$), this number and thus both Young's modulus and bending stiffness are sharply declining in all three cases; a bit less for state C than state B, and for state B than state A.

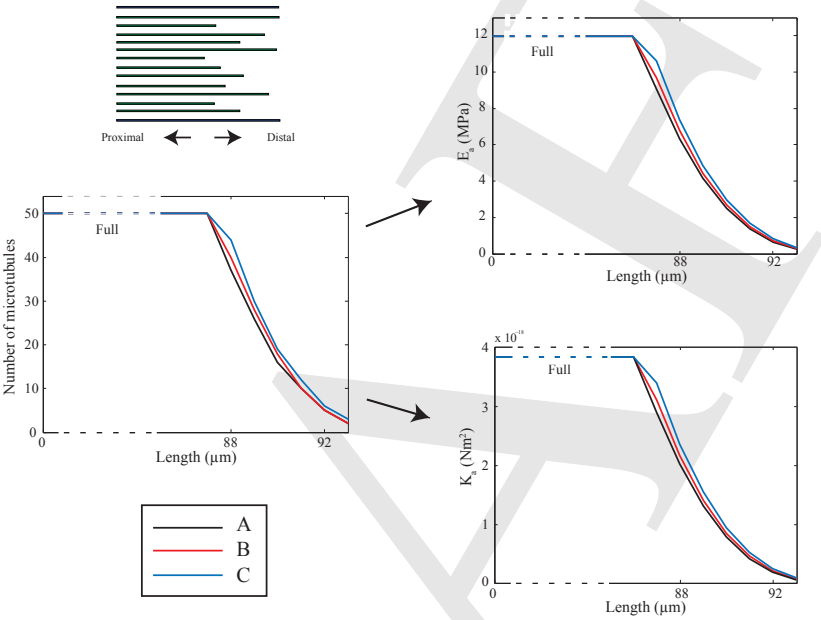

Figure 5: Mechanical properties prediction: microtubule occupancy is evaluated for tip position at A $(62,700s)$, B $(65,780s)$, and C $(71,500s)$; based on this information, the equivalent axonal Young's modulus and bending stiffness can be evaluated

5 Discussion

5.1 Calibrated parameters

Axonal length threshold for active transport: In the experimental reference used in this work (Lindsley, Kerlin, and Rising, 2003), axon differentiation is identified when the neurite length is larger than $40\mu m$, which is a factor two larger than our calibrated parameter. Other experimental work suggests that any process longer than $\sim 10-40\mu m$ will invariably become the axon (Goslin and Banker, 1989; Esch, Lemmon, and Banker, 1999). Our value ($20\mu m$) is consequently within the literature range.

Time between two motor protein emissions: A kinesin family member 5C/heavy chain of kinesin 1/kinesin light chain 1/collapsin response mediator protein 2 complex has been associated to the transport of tubulin heterodimers and oligomers to the tip of the growing axon (Conde and Cáceres, 2009). However, our parameter (2.49 hours) is much larger than what is observed for kinesin-1A, when involved in the transport of neurofilaments, i.e., of the order of 10 min (Uchida, Alami, and Brown, 2009). Nevertheless, the latter study is concerned with different observations, and is instead correlated with neurofilaments, thus impeding a direct comparison.

As a conclusion, despite a discrepancy with the provided reference, the important role of this parameter in the fitting of the experimental curve (the period for the step shaped curve) can be judged as a strong indication that the calibrated value relates adequately to its real physical value.

Vesicle GTP dimer cargo: This parameter (8×10^{-20} mol) is also difficult to compare experimentally. However diameters of the order of $50nm$ have been reported for vesicle of other proteins (Klann, Koeppl, and Reuss, 2012), which would imply between 500 and 1000 dimers per vesicle. Our calibrated parameter implies 12000 dimers, higher than this number, but within an acceptable range in view of the uncertainty of these estimations.

GTP tubulin dimers concentration in the soma: This parameter ($3 \times 10^{-5} mol.m^{-3}$) is lower by two orders of magnitude when compared to literature data (Mitchison and Kirschner, 1984; Odde, 1997; Graham, Lauchlan, and Mclean, 2006). However in these references, the used parameter is based on rather old experimental evidences, subsequently used by default as a reference. Lacking other experimental confirmation, our parameter was kept as such.

Polymerization rate constant: This parameter ($1.27 s^{-1}$) is of the same order of magnitude as in other references (Janulevicius, van Pelt, and van Ooyen, 2006).

5.2 Microtubule occupation:

Fig. 5 shows the evolution of microtubule occupation at three stages for one of the plateaux, see Fig. 4. Based on the relatively little difference between the three states, the sharp increase in growth rate immediately following state C is mainly due to the release of a new protein motor cargo. The model thus indicates a staggered axonal growth where depletion of local concentration of GTP immediately leads to an apparently stalled growth of the overall axon (state A). However, a relatively

slow growth of individual microtubules is still ongoing (see slight increase from states A to C), until another cargo reaches the microtubule tips, thus restarting the overall axonal growth.

5.3 Axonal tip stiffness

The few references studying the stiffness of axons are unfortunately generally not taking into account the spatial gradient of mechanical properties (Bernal, Pullarkat, and Melo, 2007). This reference reports an overall Young's modulus lower by two order of magnitudes. Considering the fact that the axon is tested on its whole length, the measurement provided is consequently the one corresponding to the weakest link of the axon. Additionally, it must be emphasized that the number of microtubules is unknown in this reference, making a direct comparison relatively unreliable. The drastic variation between high density microtubule (middle of the axon) and low density microtubule (close to the growth cone) regions—a factor 100 (Y.-B. Lu, Seifert, Steinhaüser, Kirchhoff, Wolburg, Guck, Janmey, Wei, Käs, , and Reichenbach, 2006; Bernal, Pullarkat, and Melo, 2007; Betz, Koch, Lu, Franze, and Käs, 2011)—confirms such hypothesis.

Finally, the references gathered in this discussion are from diverse types of neurons, animals, brain regions and cultures. The model proposed here is consequently aiming mainly at proposing a new mechanical framework that can be adapted to more accurate/complex models as needed (Aeschlimann, 2000; Zubler and Douglas, 2009; Peter and Mofrad, 2012). It can also be extended by involving many other mechanically coupled structures such as microfilaments, neurofilaments or tau proteins (Ouyang, Nauman, and Shi, 2010b).

5.4 Growth implication

Previous works have highlighted the growth cone tensile role in neurite growth and pathfinding, as well as the complex interaction of the actin/microtubule machinery inside the growth cone (Tanaka and Kirschner, 1991; Heidemann and Buxbaum, 1994; Challacombe, Snow, and Letourneau, 1996; Williamson, Gordon-Weeks, Schachner, and Taylor, 1996; Dogterom and Yurke, 1997; Aeschlimann, 2000; Gordon-Weeks, 2004; Dogterom, Kerssemakers, Romet-Lemonne, and Janson, 2005; Lee and Suter, 2008; Betz, Koch, Lu, Franze, and Käs, 2011). The local variation of mechanical properties at the tip of the axon at the junction with the growth cone consequently implies a two-step growth pattern: i) the growth cone advances leads to a tension arising in the tip of the axon, thus leading to an elongation of this tip (and only the tip), and ii) once the elongation of the tip has been sufficient to raise significantly the overall stress in the axon, the proximal region of the axon then elongates. The higher localized elongation at the tip of the axon could, in turn,

affect its microtubule assembly mechanisms as supported experimentally (Heidemann and Buxbaum, 1994). Such observation ultimately reconciliates the elements of the controversy associated to the tensile role of the growth cone, confirming the concept of "tension as secondary messenger" (Aeschlimann, 2000): whereas the growth cone by itself might indeed be a "poor tractor", its pulling on the axon and the localization of elongation in the distal part of the axon could thus provoke a local microtubule polymerization thus *indirectly* driving the axonal growth.

6 Conclusion

A new mechanical framework aimed at predicting the mechanical properties of the axon during its growth has been proposed. This model is based on diffusion/active transport based emission of GTP tubulin dimers and on their subsequent polymerization. The mechanical properties can then be extracted from the axonal elements microtubule occupancy. Most of the model parameters were taken from literature leaving only five free parameters. These parameters were calibrated against published experimental results. The simulated axonal growth curve exhibited a reasonable fit, and the extracted mechanical properties showed a sharp change in the neighborhood of the growth cone, thus providing new insights on the importance of mechanical-biochemical coupling during axonal growth and pathfinding.

Our method is specifically designed to model the influence of the chemical mechanisms on the mechanical properties. This aspect has been ignored in other complex frameworks that provide advanced models, such as CX3D. However, the coupled mechanical properties model framework proposed in this work is easily implementable in most of these models. By differentiating the "spring-components" in the axonal elements as a function of their biochemical contents—particularly in the vicinity of the growth cone—, such new mechanical framework provides an automatic way of evaluating the corresponding stiffnesses. On a final note, it must be emphasized that the smaller stiffness observed in our model close to the growth cone will lead to a higher deformation for the same force. This enhanced mechanical characterization might render current state-of-the-art axonal models more sensible to distal mechanical stimuli, and affect locally the polymerization rate at the axonal tip. Axonal growth would thus be indirectly driven by microtubule polymerization, with local axon tip elongation as the triggering mechanism.

Acknowledgement: The authors would like to thank the anonymous reviewers for helping them to enhance greatly the quality of this paper. They also acknowledge funding from the Cajal Blue Brain Project. A.J. acknowledges support from the Amarout grant from the European Union. J.M.P. also acknowledges the ressources and support provided by CeSViMa (Madrid Supercomputing Center).

References

Aeschlimann, M. (2000): *Biophysical models of axonal pathfinding*. PhD thesis, Université de Lausanne, 2000.

Baas, P.; Buster, D. (2004): Slow axonal transport and the genesis of neuronal morphology. *J. Neurobiol.*, vol. 48, pp. 3–17.

Bernal, R.; Pullarkat, P.; Melo, F. (2007): Mechanical properties of axon. *Physical Review letters*, vol. 99, pp. 018301.

Betz, T.; Koch, D.; Lu, Y.-B.; Franze, K.; Käs, J. (2011): Growth cones as soft and weak force generators. *PNAS*, vol. 108, pp. 13420–13425.

Bower, J.; Beeman, D. (1998): *The book of GENESIS: exploring realistic neural models with the GEneral Neural Simulation System New York*. Springer-Verlag.

Carnevale, N.; Hines, M. (2006): *The NEURON book*. Cambridge University Press.

Challacombe, J.; Snow, D.; Letourneau, P. (1996): Role of the cytoskeleton in growth cone motility and axonal elongation. *Seminar. Neurosci.*, vol. 8, pp. 67–80.

Conde, C.; Cáceres, A. (2009): Microtubule assembly, organization and dynamics in axons and dendrites. *Nature Reviews. Neuroscience*, vol. 10, pp. 319–332.

Dennerll, T.; Joshi, H.; Steel, V.; Buxbaum, R.; Heidemann, S. (1988): Tension and compression in the cytoskeleton of PC-12 neurites II; quantitative measurements. *The Journal of Cell Biology*, vol. 107, pp. 665–674.

Dennerll, T.; Lamoureux, P.; Buxbaum, R.; Heidemann, S. (1989): The cytomechanics of axonal elongation and retraction. *The Journal of Cell Biology*, vol. 109, pp. 3073–3083.

Dent, E.; Gertler, F. (2003): Cytoskeletal dynamics and transport in growth cone motility and axon guidance. *Neuron*, vol. 40, pp. 209–227.

Dogterom, M.; Kerssemakers, J.; Romet-Lemonne, G.; Janson, M. (2005): Force generation by dynamic microtubules. *Current Opinion in Cell Biology*, vol. 17, pp. 67–74.

Dogterom, M.; Yurke, B. (1997): Measurement of the force-velocity relation for growing microtubules. *Science*, vol. 279, pp. 856–860.

Esch, T.; Lemmon, V.; Banker, G. (1999): Local presentation of substrate molecules directs axon specification by cultured hippocampal neurons. *J. Neurosci.*, vol. 19, pp. 6417–6426.

F. Bradke, J. F.; Spira, M. (2012): Assembly of a new growth cone after axotomy: the precursor to axon regeneration. *Nature Reviews Neuroscience*, vol. 13, pp. 183–193.

Flyvbjerg, H.; Jobs, E.; Leibler, S. (1996): Kinetics of self-assembling microtubules: an "inverse problem" in biochemistry. *Proc. Natl. Acad. Sci. USA*, vol. 93, pp. 5979–5979.

Glabraith, J.; Reese, T.; Schlief, M.; Gallant, P. (1999): Slow transport of unpolymerized tubulin and polymerized neurofilament in the squid giant axon. *Proc. Natl. Acad. Sci*, vol. 96, pp. 11589–11594.

Gordon-Weeks, P. (2004): Microtubules and growth cone function. *Journal of Neurobiology*, vol. 58, pp. 70–83.

Goslin, K.; Banker, G. (1989): Experimental observations on the development of polarity by hippocampal neurons in culture. *J. Cell. Biol.*, vol. 108, pp. 1507–1516.

Graham, B.; Lauchlan, K.; Mclean, D. (2006): Dynamics of outgrowth in a continnuum model of neurite elongation. *J. Comput. Neurosci.*, vol. 20, pp. 43–60.

Graham, B.; van Ooyen, A. (2001): Compartmental models of growing neurites. *Neurocomputing*, vol. 38-40, pp. 31–36.

Graham, B.; van Ooyen, A. (2004): Transport limited effects in a model of dendritic branching. *Journal of Theoretical Biology*, vol. 230, pp. 421–432.

Graham, B.; van Ooyen, A. (2006): Mathematical modelling and numerical simulation of the morphological development of neurons. *BMC Neuroscience*, vol. 7, no. 1, pp. S9.

Hammele, M.; Zimmermann, W. (2003): Modeling oscillatory microtubule polymerization. *Phys. Rev. E*, vol. 67, pp. 021903.

Hawkins, T.; Mirigian, M.; Yasar, M.; Ross, H. (2010): Mechanics of microtubules. *Journal of Biomechanics*, vol. 43, pp. 23–30.

Heidemann, S.; Buxbaum, R. (1994): Mechanical tension as a regulator of axonal development. *NeuroToxicology*, vol. 15, pp. 95–108.

Hely, T.; Graham, B.; van Ooyen, A. (2001): A computational model of dendrite elongation and branching based on MAP2 phosphorylation. *Journal of Theoretical Biology*, vol. 210, pp. 375–384.

Janulevicius, A.; van Pelt, J.; van Ooyen, A. (2006): Compartment volume influences microtubule dynamic instability: a model study. *Biophysical Journal*, vol. 90, pp. 788–798.

Jobs, E.; Wolf, D.; Flyvbjerg, H. (1997): Modeling microtubule oscillations. *Physical Review Letters*, vol. 79, pp. 519–522.

Keith, C. (1987): Slow transport of tubulin in the neurites of differentiated PC12 cells. *Science*, pp. 337–339.

Kirschner, M.; Mitchinson, T. (1986): Beyond self-assembly: from microtubules to morphogenesis. *Cell*, vol. 45, pp. 329–342.

Klann, M.; Koeppl, H.; Reuss, M. (2012): Spatial modeling of vesicle transport and the cytoskeleton: the challendge of hitting the right road. *PLos ONE*, vol. 7, pp. e29645.

Koch, K. (1999): *Biophysics of computation. Information processing in single neurons*. Oxford University Press.

Krottje, J.; van Ooyen, A. (2007): A mathematical framework for modeling axon guidance. *Bulletin of Mathematical Biology*, vol. 69, pp. 3–31.

Lamoureux, P.; Buxbaum, R.; Heidemann, S. (1998): Axonal outgrowth of cultured neurons is not limited by growth cone competition. *Journal of Cell Science*, vol. 111, pp. 3245–3252.

Lee, A.; Suter, D. (2008): Quantitative analysis of microtubule dynamics during adhesion-mediated growth cone guidance. *Dev. Neurobi.*, vol. 68, pp. 1363–1377.

Lee, J.; Bashur, C.; Gomez, N.; Goldstein, A.; Schmidt, C. (2010): Enhanced polarization of embyonic hippocampal neurons on micron scale electrospun fibers. *J. Biomed. Mater. Res. A.*, vol. 92, pp. 1398–1406.

Li, G.; Qin, C.; Wang, L. (1995): Computer model of growth cone behavior and neuronal morphogenesis. *J. theor. Biol*, vol. 174, pp. 381–389.

Lindsley, T.; Kerlin, A.; Rising, L. (2003): Time-lapse analysis of ethanol's effects on axon growth in vitro. *Developmental Brain Reseach*, vol. 147, pp. 191–199.

Ma, Y.; Shakiryanova, D.; Vardya, I.; Popov, S. (2004): Quantitative analysis of microtubule transport in growing nerve process. *Curr. Biol.*, vol. 14, pp. 725–730.

Margolin, G.; Gregoretti, I.; Goodson, H.; Alber, M. (2006): Analysis of a microscopic stochastic model of microtubule dynamic instability. *Phys. Rev. E*, vol. 74, pp. 041920.

McGarry, J.; Prendergast, P. (2004): A three-dimensional finite element model of an adherent eukaryotic cell. *European Cells and Materials*, vol. 7, pp. 27–33.

McLean, D.; van Ooyen, A.; Graham, B. (2004): Continuum model for tubulin-driven neurite elongation. *Neurocomputing*, vol. 58-60, pp. 511–516.

Miller, M.; Samuels, D. (1996): The axon as a metabolic compartment: protein degradation, transport and maximum length of an axon. *J. theor. Biol.*, vol. 186, pp. 373–379.

Mitchison, T.; Kirschner, M. (1984): Microtubule assembly nucleated by isolated centrosomes. *Nature*, vol. 312, pp. 232–237.

Odde, D. (1997): Estimation of the diffusion-limited rate of microtubule assembly. *Biophys. J.*, vol. 73, pp. 88–96.

Ouyang, H.; Nauman, E.; Shi, R. (2010): Contribution of cytoskeletal elements to the mechanical property of axons. In *Micro/Nano Symposium (UGIM), 2010 18th Biennial University/Government/Industry*, pp. 1–5.

Ouyang, H.; Nauman, E.; Shi, R. (2010): Contribution of cytoskeletal elements to the mechanical property of axons. In *Micro/Nano Symposium (UGIM), 2010 18th Biennial University/Government/Industry*, pp. 1–5.

Pascual-Leone, A.; Amedi, A.; Fregni, F.; Merabet, L. (2005): The plastic human brain cortex. *Annual Review of Neuroscience*, vol. 28, pp. 377–401.

Peter, S.; Mofrad, M. (2012): Computational modeling of axonal microtubule bundles under tension. *Biophys. J.*, vol. 102, pp. 749–757.

Poulain, F.; Sobel, A. (2010): The microtubule network and neuronal morphogenesis: Dynamics and coordinated orchestration through multiple players. *Molecular and Cellular Neuroscience*, vol. 43, pp. 15–32.

Suresh, S. (2007): Biomechanics and biophysics of cancer cells. *Acta Biomaterialia*, vol. 3, pp. 413–438.

Tanaka, E.; Kirschner, M. (1991): Microtubule behavior in the growth cones of living neurons during axon elongation. *The Journal of Cell Biology*, vol. 115, pp. 345–363.

Twiss, J.; Fainzilber, M. (2009): Ribosomes in axons - scrounging from the neighbors? *Trends in Cell Biology*, vol. 19, pp. 236–243.

Uchida, A.; Alami, N.; Brown, A. (2009): Tight functional coupling of kinesin-1A and dynein motors in the bidirectional transport of neurofilaments. *Mol. Biol. Cell*, vol. 20, pp. 4997–5006.

van Ooyen, A.; Graham, B.; Ramakers, G. (1994): Competition for tubulin between growing neurites during development. *Neurocomputing*, vol. 38–40, pp. 73–78.

van Pelt, J.; Dityatev, A.; Uylings, H. (1997): Natural variability in the number of dendritic segments: model-based inferences about branching during neurite outgrowth. *The Journal of Comparative Neurology*, vol. 387, pp. 325–340.

van Pelt, J.; Schierwagen, A. (2004): Morphological analysis and modeling of neuronal dendrites. *Mathematical Biosciences*, vol. 188, pp. 147–155.

van Veen, M.; van Pelt, J. (1992): A model for outgrowth of branching neurites. *J. theor. Biol.*, vol. 159, pp. 1–23.

van Veen, M.; van Pelt, J. (1994): Neuritic growth rate described by modeling microtubule dynamics. *Bull Math Biol*, vol. 56, pp. 249–273.

Williamson, T.; Gordon-Weeks, P.; Schachner, M.; Taylor, J. (1996): Microtubule reorganization is obligaroty fro growth cone turning. *Proc. Natl. Acad. Sci. USA*, vol. 93, pp. 15221–15226.

Y.-B. Lu, K. F.; Seifert, G.; Steinhaüser, C.; Kirchhoff, F.; Wolburg, H.; Guck, J.; Janmey, P.; Wei, E.-Q.; Käs, J.; ; Reichenbach, A. (2006): Viscoelastic properties of individual glial cells and neurons in the CNS. *PNAS*, vol. 103, pp. 17759–17764.

Zubler, F.; Douglas, R. (2009): A framework for modeling the growth and development of neurons and networks. *Frontiers in Computational Neuroscience*, vol. 3, pp. 25.